

**Mapping Variability of Soil Water Content and Flux across 1-
1,000 m scales using the Actively Heated Fiber Optic Method**

**Chadi Sayde¹, Javier Benitez Buelga², Leonor Rodriguez-Sinobas², Laureine El
Khoury¹, Marshall English¹, Nick van de Giesen³, and John S. Selker¹**

¹Dept. of Biological & Ecological Engineering, Oregon State University, Corvallis,
OR, USA

² Dept. of Rural Engineering, Technical University of Madrid, Madrid, Spain

³Water Management Civil Engineering and Geosciences, Delft University of
Technology, Delft, Netherlands

First revision of manuscript submitted to

Water Resources Research

American Geophysical Union

22 **1. Abstract**

23 The Actively Heated Fiber Optic (AHFO) method is shown to be capable of
24 measuring soil water content several times per hour at 0.25 m spacing along cables of
25 multiple kilometers in length. AHFO is based on distributed temperature sensing
26 (DTS) observation of the heating and cooling of a buried fiber optic cable resulting
27 from an electrical impulse of energy delivered from the steel cable jacket. The results
28 presented were collected from 750 m of cable buried in three 240 m co-located
29 transects at 30, 60, and 90 cm depths in an agricultural field under center pivot
30 irrigation. The calibration curve relating soil water content to the thermal response of
31 the soil to a heat pulse of 10 W m^{-1} for 1 minute duration was developed in the lab.
32 This calibration was found applicable to the 30 and 60 cm depths cables, while the 90
33 cm depth cable illustrated the challenges presented by soil heterogeneity for this
34 technique. This method was used to map with high resolution the variability of soil
35 water content and fluxes induced by the non-uniformity of water application at the
36 surface.

37

38 **2. Introduction**

39 Soil moisture is highly variable in time and space, and is the most important factor in
40 controlling the spatio-temporal variability of surface water and energy balances
41 [*Western et al.*, 2003; 2004]. Quantification of these dynamic spatial patterns have
42 been difficult to obtain, holding back the understanding of soil moisture dynamics and
43 interacting hydrological processes [e.g., *Western et al.*, 2001, 2003; *Wilson et al.*,
44 2004].

45
46 Processes such as infiltration [*Flury et al.*, 1994; *Raats*, 2001] and plant-water
47 dynamics [*Porporato et al.*, 2004] are fundamentally controlled by soil water content
48 at the point scale. Such processes are of a particular importance in agricultural systems
49 management. Detailed information on soil moisture is needed for applications
50 including improved yield forecasting and irrigation scheduling [*Shmugge*, 1980].

51
52 *Sayde et al.* [2010] provided a laboratory demonstration of the feasibility of the
53 Actively Heated Fiber Optics (AHFO) method for distributed, 0.25-10,000 m scale
54 measurement of soil moisture content. This approach is based on observing the heating
55 and cooling of a buried fiber optic cable through the course of a pulse application of
56 energy as monitored by a distributed temperature sensing (DTS) system.

57 The ability of DTS to report the temperature each meter along fiber optic cables in
58 excess of 10,000 m in length at high temporal frequency has opened many important
59 opportunities in environmental monitoring [e.g., *Selker et al.*, 2006a; 2006b; *Tyler et*

60 *al.*, 2009], including the estimation of the surface water content and evapotranspiration
61 under suitable conditions from computing the energy balance of the soil using
62 temperature measurements at several depths [*Steele-Dunne et al.*, 2010].

63

64 The use of actively heated fiber optics for observation of subsurface water movement
65 has been mentioned previously [e.g., *Weiss*, 2003; *Perzmaier et al.*, 2004; *Aufleger et*
66 *al.*, 2005; and *Perzmaier et al.*, 2006; *Streig and Loheide*, 2012] and our team
67 demonstrated the feasibility of using AHFO for accurate distributed measurement of
68 soil water content [*Sayde et al.*, 2010]. Most recently The AHFO method has been
69 used to monitor water wetting bulbs formation around drip emitters in a laboratory
70 experiment [*Gil-Rodriguez et al.*, 2012] and water distribution inside a lysimeter
71 [*Ciocca et al.*, 2012]. In these applications the fiber optic is encased in a stainless steel
72 capillary tube surrounded by copper windings or a molded aluminum encasement, all
73 of which are enclosed in an electrical insulation sufficient for the voltage employed
74 and appropriate for direct burial. The metallic component of the fiber optic cable is
75 used as an electric resistance heater to inject heat concentric to the fiber optic sensing
76 element into the surrounding soil, while the optical fiber is used as a thermal sensor to
77 monitor the resulting temperature changes. The soil thermal properties are a function
78 of soil texture, bulk density, temperature, and soil moisture content. Under ambient
79 temperature conditions, soil moisture content can be inferred by analysis of thermal
80 responses of specific soils to the heat pulse. *Sayde et al.* [2010] presented a novel
81 approach to the interpretation of these heat pulse signals which was optimized for use

82 with DTS. Here, the thermal response of the soil is calculated in the form of an
 83 integral of the temperature increase over time in the presence of energy input, which
 84 represents the product of change in temperature and lapsed time (T_{cum}) from the start
 85 of the heat pulse. Soil moisture content is computed via T_{cum} through a calibration
 86 equation. The theory is that higher water content will reduce the change in temperature
 87 relative to drier soil, reducing this integral. This procedure yielded relatively accurate
 88 estimation of soil moisture content. *Sayde et al.* [2010] found that the absolute
 89 accuracy of the soil water content measurements varied approximately linearly with
 90 water content. At volumetric moisture content of $0.05 \text{ m}^3 \text{ m}^{-3}$ the standard deviation of
 91 the readings was $<0.01 \text{ m}^3 \text{ m}^{-3}$, and at $0.41 \text{ m}^3 \text{ m}^{-3}$ volumetric moisture content the
 92 standard deviation was $0.046 \text{ m}^3 \text{ m}^{-3}$. *Sayde et al.* [2010] indicated that this error could
 93 be further reduced by increasing the signal-to-noise ratio which could be accomplished
 94 by: averaging several heat-pulse results; using a more precise DTS unit; increasing the
 95 heating intensity; or increasing the duration of the heating. In a small scale field test of
 96 the AHFO method, *Streig and Loheide* [2012] reported a RMSE of $0.016 \text{ m}^3 \text{ m}^{-3}$ for
 97 soil moisture content $\leq 0.31 \text{ m}^3 \text{ m}^{-3}$, and a RMSE of $0.05 \text{ m}^3 \text{ m}^{-3}$ for higher soil
 98 moisture content values. The results of both experiments were obtained using DTS
 99 with approximately ten fold lower precision than those currently available, suggesting
 100 that more precise soil moisture measurements are now feasible, although calibration of
 101 the method to specific soils will be required to realize this potential.
 102 The objective of this work is to evaluate the performance and the applicability of this
 103 technology under field conditions. In this work, we test the ability of the AHFO

104 method to capture small scale (<1 m) variation in soil water content and fluxes as
105 imposed by controlled spatially variable water application at the soil surface. We will
106 also discuss methods to improve the calibration procedure and the quality of the
107 AHFO outputs.

108

109 **3. Materials and Methods**

110 **3.1 Site description**

111 The study site is located on a farm near Echo, OR. The 26 ha agricultural field was
112 irrigated by a center pivot system designed to deliver water up to 4 cm d^{-1} . The
113 spacing between consecutive emitters decreased with distance from the center while
114 their discharge rates increased, as required to ensure a spatially even application depth
115 (Appendix 1).

116

117 The field was planted with corn on March 17th, 2009 and harvested on September 15th,
118 2009. The soil is sandy loam and the average bulk density, determined from 26 non-
119 disturbed soil samples at four locations from soil surface to 90 cm depth, was 1.67 g
120 cm^{-3} with a standard deviation of 0.12 g cm^{-3} .

121

122 **3.2 Field installation and data collection procedure**

123 In October 2007, three Fiber Optic (FO) cables were installed below the tillage depth
 124 along a 240 m transect (Figure 1) at 30, 60, and 90 cm below the surface. A plow
 125 system was designed and built for this installation. The plow was made of a 2.54 cm
 126 thick steel blade with trailing-edge tubes through which the cables were introduced
 127 underneath the soil surface (Figure 2). By ganging the three tubes along the trailing
 128 edge of the plow, we installed three sets of cables at the three depths in a single pass.
 129 The most rapid possible re-establishment of native soil conditions surrounding the
 130 installed cables was critical to our considerations; therefore, the plow blade was held
 131 at a 45 degree angle from vertical, so that the weight of the soil would assist in closing
 132 the cut made in the soil. The first and the last 8 m ends of each of the three FO cables
 133 sets were submerged in an ice bath for calibration and validation of the DTS readings.
 134 The FO cable (BruSteel® manufactured by Brugg Cable, Brugg, Switzerland)
 135 deployed in the field had an outer diameter (OD) of 3.8×10^{-3} m and is composed of
 136 four optical fibers encased in a central stainless steel capillary tube (OD 1.3×10^{-3} m;
 137 inner diameter ID 1.07×10^{-3} m) surrounded by 12 stainless steel strands (OD $4.2 \times$
 138 10^{-4} m stainless steel wires), all of which were enclosed in a 7.3×10^{-4} m thick nylon
 139 jacket. The metallic components of the cable had an electrical resistance of $0.365 \Omega \text{ m}^{-1}$
 140 ¹ at 20 °C.

141

142 By splicing the end of an optical fiber at one depth to the end of an optical fiber at the
 143 following depth, The FO cables were optically connected between the three depths to

144 form a continuous optical light-path allowing simultaneous temperature reading along
145 the whole installation. A DTS unit (SensorTran DTS 5100 M4, Houston, TX),
146 connected to the FO system, recorded temperature every 0.5 m along the fiber-optic
147 cable, with a spatial resolution of 1 m for each single measurement. The average
148 temperature reading frequency was 0.2 Hz.

149

150 The high voltage power supply available at the center pivot system provided an
151 average of 490 VAC to heat one of the three sections with an average power intensity
152 of 11 W m^{-1} . A series of timers and relays insured that each of the three cable section
153 was heated separately for 1 minute duration every hour. A voltmeter located at the
154 center pivot, was employed to measure the applied voltage.

155

156 Spatial variability in soil water content and flux was imposed by varying the water
157 application pattern at the soil surface. The center pivot was programmed to repeatedly
158 pass back and forth covering a 21° angle sector of the center pivot circle such that only
159 the 3 outer sections of the cable transect (described below) were covered by the center
160 pivot path, while the section nearest the pivot was not irrigated. The center pivot
161 operation and the discharging emitters' location and spray geometry were modified to
162 apply four distinct but simultaneous water application treatments along the FO cables
163 transect location as follows:

- 164 ▪ Section 1: From 0 to 55 m radial position. No water was applied over or
165 immediately adjacent to section 1.

- 166 ▪ Section 2: From 55 to 110 m radial position. The emitters were shrouded in
167 open plastic sleeves such that water was applied directly below the emitters
168 instead of the typical circular pattern (Figure 2 of the supplementary material).
169 This insured a high application rate directly below the emitters while the inter
170 emitters locations were kept dry. The last sprinkler in section 2 (sprinkler # 19)
171 was turned off to insure separation of treatment with section 3. After 20
172 minutes from the irrigation start time, the plastic sleeve of sprinkler # 13 burst
173 and this sprinkler was turned off for the remaining of the experiment.
- 174 ▪ Section 3: Radially from 110 to 158 m. Of the 12 emitters covering this
175 section, the inner-most was turned off (to create separation of treatments); the
176 next discharged at its regular position; while the next ten were grouped into
177 five sets of paired emitters (Figure 3 of the supplementary material).
- 178 ▪ Section 4: From 158 to 240 m. Alternating application. Of the 21 emitters
179 covering this section, 10 were turned off and the remaining emitters were
180 applying water at their regular positions, either as isolated individual emitters,
181 or in pairs of emitters. (see Table 1 and Figure 4 of the supplementary
182 material).
- 183
- 184 Water was applied for 7 h. Heat pulses were applied every hour for 48 h starting 6 h
185 prior to water application.

186 **3.3 Data interpretation**

187 The heat pulse signals were interpreted using the methodology described in *Sayde et*
 188 *al.* [2010] wherein the thermal response of the soil is calculated as an integral
 189 temperature change relative to the pre-heated temperature due to energy input over
 190 time:

$$191 \qquad T_{cum} = \int_0^{t_0} \Delta T dt \qquad \text{Eq. 1}$$

192 Where T_{cum} (°C s) is the integral of ΔT (°C), the DTS reported temperature change
 193 from the pre-pulse temperature due to energy input during the total time of integration
 194 t_0 (s). The soil moisture content is inferred from T_{cum} through a calibration equation
 195 which under laboratory conditions yielded ± 1.5 % errors in estimation of soil
 196 moisture content [*Sayde et al.*, 2010].

197

198 **3.4 Lab calibration**

199 The soil specific calibration of the equation relating the thermal response (T_{cum}) to soil
 200 water content θ was obtained from a laboratory experiment. This was carried out using
 201 the same field fiber optic cable but installed in a cylindrical plastic barrel of 0.51 m
 202 diameter and 0.91 m height of repacked soil from the experimental site prepared to
 203 reproduce the average bulk density observed in the field. An outlet was installed 0.1 m
 204 above the bottom and a 0.012 m diameter perforated hose was fitted to the inside of

205 the drainage port and wound in a tight spiral which covered the bottom of barrel to
206 provide an easily controlled lower boundary condition.

207

208 Within the column, 10 m of BruSteel® FO cable in a helicoidal geometry was
209 supported by three vertical steel rods 6.4×10^{-3} m in diameter. The cable made eight
210 0.3 m diameter helical coils, spaced 0.1 m vertically, starting 0.05 m from the bottom
211 and ending at the surface of the soil (0.9 m from the bottom). The soil was collected
212 from the soil surface to the 70 cm depth at two locations near the fiber optic cable in
213 the field. The soil was air-dried before being added to the column in 20 kg lifts. After
214 each lift, the soil was compacted to the volume that corresponds to the prescribed soil
215 bulk density. No settling was observed during the experiment.

216

217 From the 17 m continuous section of the FO cable, a 4-m unheated section was placed
218 in a temperature monitored water bath for calibration and validation purposes. The
219 next 11.4 m of cable (including the section in the soil column) was heated by
220 connecting the stainless steel windings to variable voltage AC current source (Staco®
221 Variable Autotransformer Type 3PN1010). The $\sim 0.1\%$ drop in voltage along the 12
222 AWG copper connecting wires was negligible in our calculations. A digital timer with
223 a precision of $\pm 0.01\%$ (THOMAS® TRACEABLE® Countdown Controller
224 97373E70) controlled the duration of heat pulses.

225

226 The calibration data were obtained in three phases: Phase I) θ ranging from 0.23 to
227 $0.15 \text{ m}^3 \text{ m}^{-3}$; Phase II) θ ranging from 0.11 to $0.05 \text{ m}^3 \text{ m}^{-3}$; and Phase III) θ at
228 saturation ($0.40 \text{ m}^3 \text{ m}^{-3}$). The conditions for phase I were established by saturating the
229 soil column from its bottom. Then, this column was gravity drained for 3 days with its
230 top covered to reduce evaporation. At this point, DTS measurements of 6 s resolution
231 were taken during 1 minute, 10 W m^{-1} heat pulses. Three replicates with the same
232 combinations of power intensity and pulse duration were applied. Following the final
233 DTS measurements in the drained column, 14 volumetric samples were collected at
234 seven depths from the soil surface downwards to 10 cm from the column bottom.

235

236 In phase II, the top cover of the column was removed, and the column was left
237 exposed to the ambient room environment for three months to generate a smooth
238 transition from air-dry soil at the column top to nearly saturated conditions at the
239 column base. After DTS measurements, 32 soil samples were gathered for water
240 content determination. These were collected following 12.5 cm spans along the cable
241 moving from the soil surface up to 50 cm from the bottom.

242 In phase III, the remaining 50 cm of the soil column that had not yet been excavated
243 was saturated from the bottom up.

244

245 Two DTS instruments were used during the lab calibration:

- 246 • SensorTran DTS 5100 M4 in phase I: This DTS unit recorded temperature
247 every 0.5 m along the fiber-optic cable, with a spatial resolution of 1 m for

each single measurement. The average reading frequency was 0.17 Hz. The manufacturer reported temperature resolution at 2.5 km, 1 m spatial resolution, and 0.17 Hz is 0.53 °C.

- Silixa Ultima (Silixa, London, England) in phase II and III: This DTS unit recorded temperature every 0.125 m along the fiber-optic cable, with a spatial resolution of 0.29 m. The average reading frequency was 1 Hz. The manufacturer reported temperature resolution at 2.5 km, 0.29 m spatial resolution, and 1 Hz is 0.3 °C, which is consistent with the results we observed for our much shorter cable.

3.5 Thermal properties of the soil column

Measurement of soil thermal properties were made to allow comparisons of the calibration equations obtained from the lab experiments to the ones from either analytical or numerical solutions of the heat transport models. Thermal conductivity and specific heat were measured with an accuracy of 5% using a dual-needle probe (Decagon KD2-Pro® equipped with SH-1® dual-needle) in nine undisturbed soil samples and for soil water contents ranging from saturation ($0.40 \text{ m}^3 \text{ m}^{-3}$) to air-dry conditions. The nine samples were randomly chosen from the set of 14 non-disturbed soil samples used for the determination of soil water content distribution across the soil column in phase I of the lab calibration. For the air-dry conditions, the previously oven dried samples were kept exposed to ambient air for a period of two months

269 before thermal properties were measured. For the saturated conditions, the same set of
270 samples was submerged in water for 24 hours period prior to measurements. For soil
271 water content between saturation and air-dry conditions, the saturated samples were
272 placed in a pressure chamber for three days to reach equilibrium at each of the four
273 pressure levels (0.07, 0.33, 0.66, and 1.0 bar), after which soil water content was
274 determined gravimetrically and soil thermal properties measured as described above.
275 Subsequently, the samples were exposed to ambient air conditions for 48 h and then
276 covered for another 48 h before the soil water content was determined gravimetrically
277 and the soil thermal properties were measured. Finally, all the samples were oven
278 dried to 105 °C and left covered for 12 h in ambient room temperature to cool down
279 prior to the measurement of thermal properties.

280

281 **3.6 Adjusting for the variation in the applied power intensity**

282 In the field deployment, the actual applied power may vary between heat pulses due
283 to: 1) ± 2 V fluctuation in the applied voltage, and 2) thermal dependency of the
284 electrical conductivity of the FO cable's heating element (the stainless steel
285 component). For a constant resistance power is proportional to the square of applied
286 voltage, thus the fluctuation on the nominal 480 V supply contributed to a 0.9%
287 uncertainty in the applied energy. Changes in the electrical resistance of the FO
288 heating element were a function of the cable temperature. Thus, it could be accurately
289 estimated via the DTS measured cable temperature.

290
 291 Since the soil thermal heat flow and heat storage processes in this system are linear,
 292 the temperature increase, and in consequence value of T_{cum} , are proportional to the
 293 power applied, as seen in both the cylindrical source transient and the line source
 294 transient methods [see *Blackwell*, 1954; *de Vries and Peck*, 1958; *Jaeger*, 1965;
 295 *Shiozawa and Campbell*, 1990; *Bristow et al.*, 1994]. Thus the effects of temporal
 296 variation in the power can be eliminated by linearly scaling observed temperatures to
 297 those that would have been obtained at a common reference power intensity.

298

299 **3.7 Calculating water front travel time**

300 To compare the soil water content response for the different wetting regimes in the
 301 field, a time-lagged cross-correlation analysis was performed between the time series
 302 of soil moisture change at each particular position along the FO cable installed at 30
 303 cm depth and those of its corresponding position along the FO cable at the 60 cm
 304 depth. The cross-correlation method has been employed successfully to study time-lag
 305 relationship between soil moisture content at variable depths [*Georgakakos et al.*,
 306 1995; *Mahmood and Hubbard*, 2007; *Mahmood et al.*, 2012].

307

308 The Matlab function “Xcorr” was used to calculate the cross-correlation coefficient,

309 $\hat{R}_{xy}(m)$, associated with each time lag (m) tested as follows:

$$\hat{R}_{xy}(m) = \begin{cases} \sum_{n=0}^{N-m-1} x_{n+m} y_n & m \geq 0 \\ \hat{R}_{yx}(-m) & m < 0 \end{cases} \quad \text{Eq. 2}$$

310 Here x and y are soil water content at the 30 and the 60 cm depth, normalized by their
 311 initial value ($m = 0$). N is the length of the x and y vectors.
 312 The maximum correlation coefficients value is used to identify the appropriate time
 313 lag to represent the wetting-front travel time at each location (see Table 2 in the
 314 supplementary material for a list of maximum correlation coefficient per location and
 315 its corresponding time lag value).

316 3.8 Calculating Water Fluxes

317 For each particular location (i) along the fiber optic cables and for each particular
 318 depth (d) a wetting front velocity (V_{id}) and a flux (F_{id}) can be calculated as follows:

$$319 \quad V_{id} = D_{id} l_{id}^{-1} \quad \text{Eq. 3}$$

320 and

$$321 \quad F_{id} = V_{id} \Delta\theta_{max_{id}} \quad \text{Eq. 4}$$

322

323 Where:

- 324 ▪ D_{id} is the distance between two successive depths, $D_{id} = 30$ cm in our case,
- 325 ▪ l_{id} is the time period elapsed between the wetting front arrival at two
- 326 successive depths (h),
- 327 ▪ $\Delta\theta_{max_{id}}$ is the maximum change in volumetric water content ($\text{m}^3 \text{m}^{-3}$).

328

329 **3.9 Assessing the impact of the convective heat transfer from moving water**

330 The calibration equation to translate T_{cum} measurements into soil water contents was
 331 developed in the laboratory under hydrostatic conditions. One concern is the validity of
 332 this calibration curve under convective heat transfer conditions from moving water i.e.
 333 when water infiltrates at a velocity that is significant in comparison to the velocity of
 334 the heating front. A common practice to assess if the convective heat transfer from
 335 moving fluid can be omitted from the heat transfer calculation is to evaluate the Peclet
 336 number (Pe). Pe compares the relative strength of convective to diffusive transport of
 337 the same physical quantity, applicable to heat and mass transport processes. The
 338 critical value of Pe depends upon the application. It is common to employ the criteria
 339 of $Pe < 1$ to delineate transport processes dominated by diffusion (e.g.,
 340 ONDRAF/NIRAS, 2002 as cited in *Huysmans and Dassargues*, 2004). However, this
 341 is not universal, for instance *de Marsily* (1986) took mass transport processes to be
 342 controlled by diffusion for $Pe < 2$. *Wilson et al.* (1993) took the transition between
 343 diffusion controlled and advection controlled mass transport to occur $1.5 < Pe < 15$ (as
 344 cited in *Huysmans and Dassargues*, 2004). We will take the most conservative value
 345 since we seek to identify where the laboratory diffusion-only results are applicable to
 346 the field, and assume that diffusion dominates for $Pe < 1$.

347

348 For heat transfer in porous media, Pe can be calculated as (*Bear*, 1972; *Hopmans et*
 349 *al.*, 2002):

$$Pe = V_{conv}L/\kappa \quad \text{Eq. 5}$$

with

$$V_{conv} = v \theta C_w / C_{bulk} \quad \text{Eq. 6}$$

Where

Where V_{conv} is the convective heat pulse velocity in a porous media (m s^{-1}) i.e. the heat flow by the moving liquid phase, v is the average pore water velocity (m s^{-1}), θ is the soil volumetric water content ($\text{m}^3 \text{ m}^{-3}$), C_w is the water volumetric heat capacity ($\text{J m}^{-3} \text{ K}^{-1}$), C_{bulk} the soil volumetric heat capacity ($\text{J m}^{-3} \text{ K}^{-1}$), and L is the characteristic length (m). For a heat pulse probe application, *Hopmans et al.* [2002] defined L as being the characteristics length of the porous media approximated by the medium grain size. We will follow a more conservative approach here and define L as the effective distance traveled by the convective water front during the heating time t ($t=60$ s in our case) such as:

$$L = v t \theta \quad \text{Eq. 7}$$

Substituting V_{conv} by (2) and L by (3) in (1) we get:

$$Pe = (v \theta)^2 t C_w / (C_{bulk} \kappa) \quad \text{Eq. 8}$$

368 **4. Results**

369 **4.1 Lab calibration results and system performance**

370 A calibration equation was fitted to the data relating measured soil water content to
 371 measured T_{cum} (Figure 3). The gravimetric samples from the soil column had an
 372 average bulk density (ρ_b) of 1.63 g cm^{-3} with a standard deviation (σ_b) of 0.06 g cm^{-3} ,
 373 in the range of values found in the field ($\rho_b=1.67 \text{ g cm}^{-3}$ and $\sigma_b=0.12 \text{ g cm}^{-3}$) and those
 374 published for this soil by the Natural Resources Conservation Service NRCS (1.15--
 375 1.70 g cm^{-3} range; Table 1).

376

377 T_{cum} became insensitive to variation in soil water content at high water content ($S >$
 378 0.4 ; Figure 3). The shape of the calibration curve for very dry soil conditions (e.g., $S <$
 379 0.1) also suggests that T_{cum} is insensitive to variation in soil water content in this
 380 range. In the later case, this can be explained by observing the behavior of the soil
 381 thermal conductivity (λ) at low soil water content. In fact, λ has been shown to be
 382 nearly constant from water contents ranging from zero to a critical value (θ_{cr}) (Figure
 383 4a). This could be explained by the water geometry transitions from pendular to
 384 funicular [*de Vries*, 1963; *Tarnawski and Leong*, 2000]. The value of θ_{cr} tends to be
 385 dependent on the clay content of the soil [*Tarnawski and Leong*, 2000; *McInnes*,
 386 1981]. The observed θ_{cr} value ($0.03 \text{ m}^3 \text{ m}^{-3}$) is in agreement with *de Vries*' [1963]
 387 recommendation of using θ_{cr} values of $0.03 \text{ m}^3 \text{ m}^{-3}$ for coarse soils. This behavior is
 388 also observed in the thermal diffusivity curve (Figure 4b).

389 For soil water content ranging from 0.04 to 0.40 m³ m⁻³ (0.1 < S < 1) the slope in the
 390 relationship relating θ to T_{cum} decreases with soil water content (Figure 3) indicating
 391 that error in soil water content estimation is expected to increase with increasing soil
 392 water content as observed in *Sayde et al.* [2010] and *Gil-Rodriguez et al.* [2012].
 393 The error in T_{cum} , σ_{Tcum} , was determined by measuring the variability in T_{cum} over
 394 repeated measurements at constant soil moisture content, as in *Sayde et al.* [2010].
 395 Under the lab conditions, with a Silixa Ultima-S, 85% of the variability in σ_{Tcum} (3.18
 396 °C s) was due to instrument noise when 1s and 0.12 m sampling resolutions were
 397 employed. The remaining 15% is believed to have been caused by voltage fluctuation
 398 during heating and spatial variability of soil thermal properties in the soil column.
 399 However, the noise in T_{cum} obtained with the SensorTran 5100 unit was 12.6 °Cs for
 400 the 6 s and 0.5 m sampling resolutions conditions, a level at which any other source of
 401 error was undetectable. The maximum error in soil water content determination was
 402 observed at saturation (Figure 5). This error was 0.03 m³ m⁻³ and 0.11 m³ m⁻³ for the
 403 Silixa Ultima-S and the SensorTran 5100, respectively.

404 **4.2 Field test results**

405 **4.2.1 Soil water content**

406 The calibration equation developed in section 2 (Figure 3), was used to translate T_{cum}
 407 values observed over the three depths cables in the field to soil water content. The
 408 slope of the calibration curve is high for near saturated soil and low at low soil water
 409 content. As pointed out by *Sayde et al.* [2010] this implies the method is less sensitive

410 in wet conditions. Furthermore, if for any reason the values of T_{cum} are biased low,
411 then it is possible to compute values that are not in the range of the calibration results,
412 and therefore yield undefined soil moisture. On the other hand, if the calibration curve
413 is biased high, then the soil moisture estimates from T_{cum} will not include high water
414 contents.

415

416 The 90 cm depth soil water contents, as estimated using the calibration curve of Figure
417 3, clearly showed the characteristics of a high- bias. Though the changes in T_{cum} at the
418 90 cm depth were of same magnitude and with similar spatial patterns as those
419 observed at the 30 and the 60 cm depths (Figure 6), these did not result in significant
420 soil water content changes as were observed with the 30 and the 60 cm depths. The
421 calibration challenges are discussed with further details in section 5.

422 The 30 and the 60 cm DTS estimated soil water content corresponded to those
423 expected from the four patterns of spatial variability imposed at the soil surface.
424 Section 1 (between 0 and 55 m) was not irrigated, and as expected, no significant
425 water change was detected at either depth (Figure 7 and 8). Between 55 and 110 m
426 (Section 2), the nine constraining sleeves imposed high-rate (0.35 l s^{-1}) water
427 application directly below each emitter, as seen at the nine locations with high soil
428 water content change in this section (Figure 7 and 8). The average total water applied
429 over the nine wetted locations was 72 mm. In section 3 (between 110 m and 158 m),
430 the four wide strips of high soil water content change observed at both 30 and 60 cm
431 depths (Figure 7 and 8) correspond to the expected patterning of the paired emitters.

432 In section 4 (from 158 m to the end), at the 30 cm depth the highest soil water content
 433 increases were observed at the locations of the operating emitters (Figure 8a). For the
 434 60 cm depth cable, the pattern was the same but the variation in soil water content was
 435 more modest than under the other treatments (Figure 8b), as expected due to the lower
 436 water application. The average total water applied over section 4 was 32 mm while
 437 this value was 72 mm and 54 mm over the wetted locations of section 2 and section 3
 438 respectively.

439

440 **4.2.2 Soil Water flux density**

441 To calculate the water front travel time from depth 30 cm to depth 60 cm, the data
 442 obtained along the fiber optic cable were separated into two groups based on the
 443 maximum change in soil water content observed at the 30 cm depth locations. The first
 444 group of data represents data retrieved from locations where $\Delta\theta > 0.05 \text{ m}^3 \text{ m}^{-3}$ at the
 445 30 cm depth, with the second group being the remaining locations (see Figure 9a).

446 For the first group, the average time lags were 0.64 h (standard deviation of 0.97 h),
 447 2.55 h (standard deviation of 1.21 h), and 3.46 h (standard deviation of 2.91 h) for
 448 sections 2, 3, and 4, respectively. This variation follows the pattern of water
 449 application at the soil surface for the three treatment sections: section 2 received the
 450 highest application rate for all locations in group 1, and section 4 the lowest
 451 application rate.

452

453 The same method was used to calculate the wetting front travel time from depth 60 cm
 454 to depth 90 cm. Since the T_{cum} to moisture content calibration developed for the upper
 455 soil was observed unsuitable for the 90 cm depth, the time series of change in T_{cum}
 456 (from pre-irrigation conditions) for both 60 and 90 cm depths are employed instead of
 457 the time series of change in soil water content. As before, the calculated time lag was
 458 separated into two groups; Group 1 includes the time lag for location where $\Delta\theta$ at 60
 459 cm was $> 0.05 \text{ m}^3 \text{ m}^{-3}$, and Group 2 for where $\Delta\theta$ at 60 cm was $< 0.05 \text{ m}^3 \text{ m}^{-3}$ (Figure
 460 9b). For the Group 1, the average time lags were 0.93 h (standard deviation of 1.72 h),
 461 3.33 h (standard deviation of 1.49 h), and 5.89 h (standard deviation of 1.83 h) for
 462 sections 2, 3, and 4, respectively. On average, the wetting front movement was 32%
 463 faster between the 30 and the 60 cm depths than between the 60 and the 90 cm depths.

464
 465 Readers should be aware of the high uncertainty associated with the use of the time lag
 466 to estimates the wetting front traveling time for section 2 of the fiber optic cable
 467 location. In section 2, about half of the time lag values calculated for the different
 468 positions at the 30 cm depth and for a lesser extent at the 60 cm depth have either
 469 negative or zero values. This is a clear indication that the transit times were not long
 470 enough to be accurately quantified based on 1-h measurement intervals between
 471 moisture content measurements at the highest fluxes. Thus, the results of section 2
 472 were considered non-reliable to estimate the water front traveling time and will not be
 473 used in the further analysis.

474

475 The estimates of the wetting front traveling times in sections 3 and 4 allow calculation
 476 of the wetting front velocity and associated flux.

477

478 As expected, larger water fluxes were computed below the locations that showed
 479 higher increase in water content (Figure 10, and Table 2), which in turn are associated
 480 with the locations of the discharging emitters as discussed in a previous section. The
 481 fluxes diminish with depth following the pattern of water application. Average flux
 482 was reduced by 41% over section 3, and 71% over section 4 (see Table 2). This was
 483 expected in section 3 compared to section 4, as the applied discharge rate was the
 484 highest, and localized over a smaller wetted area.

485

486 To assess if the convective heat transfer from moving water in the soil was large
 487 enough to bias $T_{cum}-\theta$ calibration, an average Pe was calculated for each section. For
 488 section 3, the average time lag observed over the locations with $\Delta\theta > 0.05 \text{ m}^3 \text{ m}^{-3}$ was
 489 2.55 hr between the 30cm and 60cm depths and 3.3 hr between the 60cm and 90cm
 490 depths (an average time lag of 2.9 hr over all depths). For section 4, the average time
 491 lag observed over the locations with $\Delta\theta > 0.05 \text{ m}^3 \text{ m}^{-3}$ was 3.64 hr between the 30 cm
 492 and 60 cm depths and 5.89 hr between the 60 cm and 90 cm depths (an average time
 493 lag of 4.8 hr over all depths). This yields an average water front velocity of 0.029 mm
 494 s^{-1} for section 3 and 0.017 mm s^{-1} for section 4. For each of these velocities, Equation
 495 8 was used to calculate Pe . The values for k were obtained from the laboratory
 496 measurements described in section 3.5 (see Figure 4b). Equation 8 yielded $Pe= 0.013$

497 for section 3, and $Pe = 0.0048$ for section 4. Even for section 2 where the water front
 498 velocity was considered overestimated and unreliable $Pe = 0.18$. These results indicate
 499 that the effect of the flowing water convective heat transfer on the T_{cum} based
 500 estimated θ can be considered negligible for the conditions of these experiments.

501

502 **5. Discussion**

503 The calibration relating DTS measured T_{cum} to soil water content (Figure 3) was
 504 determined in a rather laborious laboratory experiment. The soil column was only
 505 representative of the top 70 cm of the soil, the maximum depth in the field from which
 506 soil was collected. In keeping with unpublished observations of a textural transition
 507 observed during the installation of neutron probe tubes, beyond 70 cm depth the soil
 508 had different thermal properties and thus the calibration equation obtained in
 509 laboratory experiment was not directly applicable to the 90 cm depth cable. These
 510 results illustrate that a more practical calibration methodology will be needed for the
 511 method to find broad adoption, and ideally this would be an in situ approach given the
 512 complexity of typical soils.

513 Another disadvantage of the calibration conducted in laboratory that even if the soil
 514 was collected in situ and repacked to original bulk density, it has been disturbed
 515 during this process. In this case, the grain to grain contact might be different which
 516 can also affect the water bridges formations. The soil restructuring can lead to
 517 deviation in the measured thermal properties of the soil. That said, this experiment was
 518 conducted in an agricultural field that was subject to periodic plowing up to 90 cm

519 depth. The effect of this plowing process and the post plowing soil recovery on
520 homogenizing the plowed profile and reshuffling the grain to grain contact is expected
521 to be of similar magnitude of preparing the soil column in the laboratory.

522

523 The most direct, although time intensive, calibration method is to simultaneously
524 measure T_{cum} and soil moisture content over the full range of soil moisture conditions
525 at as many locations as there are differing soil conditions and then use the water
526 content and T_{cum} values as in Figure 3. Alternatively one could measure thermal
527 conductivity, diffusivity and water content over the full range of soil moisture
528 conditions either in the field or in undisturbed soil samples (similar to figure 4) at as
529 many locations as there are differing soil conditions. One could then use heat transport
530 numerical simulation models to generate calibration curve relating T_{cum} to soil water
531 content for that particular cable and soil. In either case, measuring thermal properties
532 of soil and soil water content over the full range of soil water content at all location
533 presents a daunting challenge.

534

535 Practical insights can be gained from looking at the relationship between thermal
536 conductivity (λ) and soil water content (θ). Most models relating λ to θ assume that the
537 fundamental shape is universal, and simply scaled for each soil [Johansen 1975;
538 Campbell 1985; Cote and Konrad 2005; Lu et al. 2006]. The scaling parameters are
539 generally obtained by optimizing the model fit to λ and θ measurements. For the

540 model described by *Campbell* [1985] one only needs a value for measurements of bulk
 541 density and two measurements of λ for wet and dry conditions.

542

543 In principle, calibration curves relating T_{cum} to soil water content would be expected to
 544 share the same basic shape; steep slope toward high water content and flat toward low
 545 soil water content, as observed in this work, in *Sayde et al.* [2010], and in *Gil-*
 546 *Rodriguez et al.*, [2012]. This suggests that calibration curves for different soil types
 547 could be scaled from few reference curves using measurements from the field
 548 representing end members of water content. The only fundamental difference in shape
 549 that we might expect between curves of different soil types is the θ_{cr} value below
 550 which T_{cum} is held nearly constant (see section 4.1).

551

552 Another factor that will significantly impact the measurements' quality using the
 553 AHFO method is the DTS instrument performance. The two instruments employed in
 554 this study resulted in a 3.5 times difference in the determination of soil moisture error
 555 (Figure 5) for the same heat pulse characteristics and soil water conditions. The large
 556 difference in measurements' quality is due to the instruments temperature
 557 measurement error. This error was computed for the instruments' finest spatial
 558 resolution, which differed between the instruments (see section 3.4 for more details).
 559 Note that the DTS reported temperature is calculated from the ratio of the magnitudes
 560 of anti-Stokes to Stokes scattered light, which are a function of total number of
 561 reflected photons. By the law of large numbers, the number of observed photons

562 follows a normal distribution with a standard deviation decreasing by the square root
563 of the total number of photons observed [Selker *et al.*, 2006a]. Since the number of
564 photons observed is a 1:1 function of the fiber volume from which photons are
565 scattered, the noise level is inversely proportional to the square root of the
566 measurement spatial length (see Selker *et al.*, 2006 for more details). If the spatial
567 resolution for both DTS instruments used in this work is set equal, the error in soil
568 moisture determination would have decreased by an additional factor of two when
569 employing the higher performance Silixa Ultima-S DTS.

570

571 Other factors may also impact the quality of the DTS measurements such as the
572 temporal drift of the soil temperature due to the diurnal temperature cycle or water
573 fluxes propagation through the soil. One way to evaluate the impact of the temporal
574 variability of the soil temperature is to look at the soil temperature temporal trend
575 during a 5 min period directly before the start of the heat pulse. For each heat pulse,
576 the average slope for the linear regression of temperature vs. time for this 5 min period
577 has been calculated for each of the four sections. The highest deviation from zero
578 slope was $-0.44 \cdot 10^{-3} \text{ }^{\circ}\text{C s}^{-1}$. It was observed at 1 hour before the start of irrigation in
579 section 4. Over a heating period of 60 s, this slope value might have caused a drop of
580 $0.0264 \text{ }^{\circ}\text{C}$ in the soil temperature which is equivalent to less than 5% of the instrument
581 noise i.e. in this experiment the effect of the soil temperature temporal variability is
582 negligible when compared to overall instrument error.

583

584 **6. Conclusions**

585 AHFO method is capable of capturing a complex spatial pattern of soil water content,
586 reporting from many hundreds of points simultaneously. These data, for instance,
587 allowed estimation of local soil water flux. delineation of these patterns with point-
588 measurement instruments would not be feasible. Larger scale measurements
589 techniques, such as Cosmic-Ray probes [Zreda *et al.*, 2008] and remote sensing, might
590 be able to provide an average picture of the change in soil water content, but, do not
591 capture the 1-1000 m scale processes observed in this experiment which are of
592 importance in irrigated agriculture, and natural systems (e.g. preferential flows and
593 contaminant transport).

594
595 The results showed that soil moisture contents and fluxes can be measured and
596 monitored at a range of values (ranging from dry to saturated conditions) that is
597 significantly larger than the <0.06 range $\text{m}^3 \text{m}^{-3}$ reported by Weiss [2003] and more
598 informative than the qualitative “dry, wet or saturated” assessment reported by
599 Perzlsmaier *et al.* [2004; 2006]. This improvement is mainly due to the use of a data
600 interpretation method (i.e. *The time integral of temperature deviation* developed by
601 Sayde *et al.* [2010]) that is appropriate to the DTS method wherein precision of
602 temperature reporting is a direct function of the interval of photon integration.

603
604 AHFO applications allow operator control over the heat signal that is injected into the
605 soil. At the expense of added power and complexity, this provides certain advantages

606 over the diurnal cycle driven heat signal employed by the passive distributed
 607 temperature sensing method for soil moisture estimation described by *Steele-Dunne et*
 608 *al.* [2010]. Specifically, it may be applied at any depth and any time whereas the
 609 passive heat signal attenuates with depth so that it is generally only applicable <30 cm
 610 depth under conditions of significant diurnal heat flux (e.g. not under dense vegetative
 611 canopy, or on cloudy or winter days).

612

613 Error in soil water content estimates due to instrumentation was reduced considerably
 614 (from 0.11 to 0.03 m³ m⁻³ at saturation) when a DTS with better performance was
 615 employed in the laboratory experiment. A generally applicable Peclet Number
 616 approach showed that water content estimates were shown to be independent of soil-
 617 water flux for the conditions employed here.

618

619 The calibration of the AHFO method remains challenging. Though yet to be
 620 developed, in principle, a calibration procedure could take advantage of the expected
 621 similarity between the relationships between T_{cum} and θ to that of thermal conductivity
 622 and θ .

623

624 **7. Acknowledgements**

625 The authors gratefully thank Kent Madison and Madison farm for their tremendous
 626 support during the installation and operation of the Fiber Optic system at their farm.

627 The authors also thank Richard Cuenca, and Scott Tyler for their helpful conversations
 628 about this experiment, and Maria Gil Rodriguez for helping in preparation of the
 629 matlab scripts. We gratefully acknowledge the support of the National Science
 630 Foundation (grant 1129003), NASA (grant NASA 10-THP-0054) and the Oregon
 631 Experiment Station for their critical financial support. We appreciate the editor,
 632 associate editor, and three anonymous reviewers' dedication to understanding the
 633 contents of this work, resulting in comments and questions that greatly improved the
 634 final manuscript.

635

636 **8. References**

- 637 Aufleger, M., M. Conrad, S. Perzlmaier, and P. Porras (2005), Improving a Fiber
 638 Optics tool for monitoring leakage, *Hydro Review Worldwide*, 13(4):18-23.
 639
- 640 Blackwell, J.H. (1954), A transient-flow method for determination of thermal
 641 constants of insulating materials in bulk, *J. Appl. Phys.*, Vol. 25, pp. 137–144.
 642
- 643 Blöschl, G., and M. Sivapalan, (1995), Scale issues in hydrological modeling: a
 644 review, *Hydrological Processes* 9:251-290.
 645
- 646 Bristow, K.L., R.D. White, and G.J. Kluitenberg (1994), Comparison of single and
 647 dual probes for measuring soil thermal properties with transient heating,
 648 *Australian Journal of Soil Research*, 32:447-464.

649

650 Campbell, G.S. (1985), Soil Physics with BASIC, Elsevier: New York.

651

652 Cote, J., and J.M. Konrad (2005), Thermal conductivity of base-course materials,

653 *Canadian Geotechnical Journal*, 42:61-78.

654

655 Farouki, O.T. (1986), Thermal properties of soils. Series on rock and soil mechanics,

656 Vol. 11, *Trans Tech Publications*, Clausthal-Zellerfeld, Germany.

657

658 Flury, M., H. Flüeler, W.A. Jury, and J. Leuenberger (1994), Susceptibility of soils to

659 preferential flow of water: a field study, *Water Resour. Res.* 30, 1945–1954.

660

661 Georgakakos, K. P., D.-H. Bae, and D.R. Cayan (1995), Hydroclimatology of

662 continental watersheds: 1. Temporal analyses, *Water Resour. Res.*, 31(3), 655-

663 675.

664

665 Hausner, M.B., F. Suárez, K. E. Glander, N. van de Giesen, J.S. Selker and S.W. Tyler

666 (2011), Calibrating Single-Ended Fiber-Optic Raman Spectra Distributed

667 Temperature Sensing Data, *Sensors*, DOI:10.3390/s111110859.

668

- 669 Jaeger, J.C. (1965), Application of the theory of heat conduction to geothermal
 670 measurements, In 'Terrestrial Heat Flow.' (Ed. W. H. K. Lee.) *American*
 671 *Geophysical Union Monograph*, Vol. 8, pp. 7-23.
 672
- 673 Johansen, O. (1975), Thermal conductivity of soils, Ph.D. thesis, University of
 674 Trondheim, Trondheim, Norway, US Army Corps of Engineers, Cold Regions
 675 Research and Engineering Laboratory, Hanover, N.H. CRREL, Draft English
 676 Translation 637.
 677
- 678 Lu, H., C.J. Moran, and I.P. Prosser (2006), Modeling sediment delivery ratio over the
 679 Murray Darling Basin, *Environmental Modeling and Software* 21:1297–308.
 680
- 681 Mahmood. R., and K.G. Hubbard (2007), Relationship between soil moisture of near
 682 surface and multiple depths of the root zone under heterogeneous land uses and
 683 varying hydroclimatic conditions, *Hydrological Processes*, 21(25):3449-3462.
 684
- 685 Mahmood R., A. Littell, K.G. Hubbard , and J. You (2012), Observed data-based
 686 assessment of relationships among soil moisture at various depths,
 687 precipitation, and temperature, *Applied Geography* 34:255-264.
 688
- 689 McInnes, K.J. (1981), Thermal conductivities of soils from dryland wheat regions of
 690 Eastern Washington, MS Thesis, Washington State Univ., Pullman, WA.

- 691
- 692 Perzlmaier, S., M. Aufleger, and M. Conrad (2004), Distributed fiber optic
- 693 temperature measurements in hydraulic engineering. - Prospects of the heat-up
- 694 method, In: Proceedings of the 72nd ICOLD Annual Meeting - Workshop on
- 695 Dam Safety Problems and Solutions-Sharing Experience, Seoul, South Korea,
- 696 May 16-22, 2004, Korean National Committee on Large Dams (KNCOLD),
- 697 Seoul, p.31.
- 698
- 699 Perzlmaier, S., K.-H. Straßer, Th. Strobl, and M. Aufleger (2006), Integral seepage
- 700 monitoring on open channel embankment dams by the DFOT heat pulse
- 701 method, Proceedings of the 22nd Congress of the International Commission on
- 702 Large Dams, Barcelona, Spain. Q. 86 – R. 12, p 145-164.
- 703
- 704 Porporato, A., E. Daly, and I. Rodríguez-Iturbe (2004), Soil water balance and
- 705 ecosystem response to climate change, *American Naturalist*, 164 (5):625–633.
- 706
- 707 Raats, P.A.C. (2001), Developments in soil–water physics since the mid 1960s,
- 708 *Geoderma*, 100:355–387.
- 709
- 710 Sayde. C., C. Gregory, M. Gil-Rodriguez, N. Tufillaro, S. Tyler, N. van de Giesen, M.
- 711 English, R. Cuenca, and J.S. Selker (2010), Feasibility of soil moisture
- 712 monitoring with heated fiber optics, *Water Resources Research*, 46, W06201,

- 713 doi:10.1029/2009WR007846.
- 714
- 715 Shiozawa, S., and G.S. Campbell (1990), Soil thermal conductivity, *Remote Sens.*
- 716 *Rev.*, 5:301–310.
- 717
- 718 Selker, J.S., L. Thévenaz, H. Huwald, A. Mallet, W. Luxemburg, N. van de Giesen,
- 719 M. Stejskal, J. Zeman, M. Westhoff, and M.B. Parlange (2006a), Distributed
- 720 Fiber Optic Temperature Sensing for Hydrologic Systems, *Wat. Resour. Res.*,
- 721 42, W12202, doi:10.1029/2006WR005326.
- 722
- 723 Selker, J.S., N. van de Giesen, M. Westhoff, W. Luxemburg, and M.B. Parlange
- 724 (2006b), Fiber optics opens window on stream dynamics, *Geophysical*
- 725 *Research Letters*, 33, L24401, doi:10.1029/2006GL027979.
- 726
- 727 Schmugge, T.J. (1980), Effect of texture on microwave emission from soils, *IEEE*
- 728 *Trans. Geosci. Remote Sens.*, GE-18:353-361.
- 729
- 730 Steel-Dunne, S.C., M.M. Rutten, D.M. Krzeminska, M. Hausner, S.W. Tyler, J.S.
- 731 Selker, T.A. Bogaard, and N.C. van de Giesen (2010), Feasibility of soil
- 732 moisture estimation using passive distributed temperature sensing, *Water*
- 733 *Resour. Res.*, 46, W03534, doi:10.1029/2009WR008272.
- 734

- 735 Strieg, A.M., and S.P Loheide II (2012), Heated distributed temperature sensing for
736 field scale soil moisture monitoring, *Ground Water*, 50 (3):340-347.
737
- 738 Tarnawski V.R., and W.H. Leong (2000), Thermal conductivity of soils at very low
739 moisture content and moderate temperatures, *Transport in Porous Media*,
740 41(2):137-147.
741
- 742 Tyler, S.W., J.S. Selker, M.B. Hausner, C.E. Hatch, T. Torgersen, C.E. Thodal, and G.
743 Schladow (2009), Environmental temperature sensing using raman spectra
744 DTS fiber-optic methods, *Wat. Resour. Res.*, doi:10.1029/2008WR007052.
745
- 746 van de Giesen, N., S. Steele-Dunne, J. Jansen, O. Hoes, M.B. Hausner, S.W. Tyler,
747 and J.S. Selker (2012), Double-Ended Calibration of Fiber-Optic Raman
748 Spectra Distributed Temperature Sensing Data. *Sensors*, 12(5), 5471-5485,
749 doi:10.3390/s120505471.
750
- 751 de Vries, D.A., and A.J. Peck (1958), On the cylindrical probe method of measuring
752 thermal conductivity with special reference to soils. Part 1. Extension of theory
753 and discussion of probe characteristics, *Aust. J. Phys.*, 11: 255-71.
754
- 755 de Vries, D.A. (1963), Thermal properties of soils. *Physics of Plant Environment*. Ed.
756 W.R. Van Wijk., 210-35. North-Holland: Amsterdam.

757

758 Weiss, J.D. (2003), Using fiber optics to detect moisture intrusion into a landfill cap
759 consisting of a vegetative soil barrier, *J. Air & Waste Manage. Assoc.*,
760 53:1130-1148.

761

762 Western A.W., G. Blöschl G, and R.B. Grayson (2001), Towards capturing
763 hydrologically significant connectivity in spatial patterns, *Water Resour. Res.*
764 37:83–97.

765

766 Western, A.W., R.B. Grayson, and G. Blöschl (2002), Scaling of soil moisture: A
767 hydrologic perspective, *Annu. Rev. Earth Planet. Sc.*, 30:149-180.

768

769 Western, A.W., S. Zhou, R.B. Grayson, T.A. McMahon, G. Blöschl, and D.J. Wilson
770 (2004), Spatial correlation of soil moisture in small catchments and its
771 relationship to dominant spatial hydrological processes, *Journal of Hydrology*,
772 286:113–134.

773

774 Wilson, J.D., A.W. Western, and R.B. Grayson (2004), Identifying and quantifying
775 sources of variability in temporal and spatial soil moisture observations, *Water*
776 *Resources Research* 40, W02507.

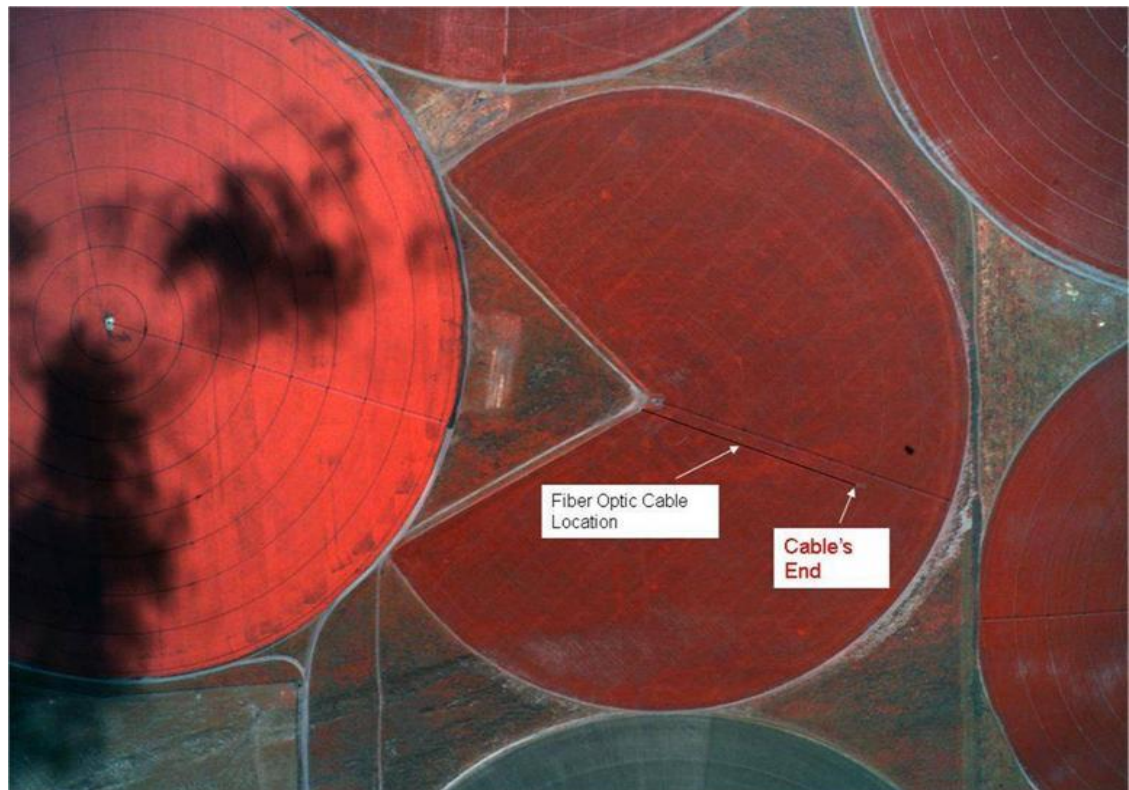
777

778 Zreda, M., D. Desilets, T.P.A. Ferré, and R.L. Scott (2008), Measuring soil moisture
779 content non-invasively at intermediate spatial scale using cosmic-ray neutrons,
780 *Geophys. Res. Lett.*, 35, L21402.

781

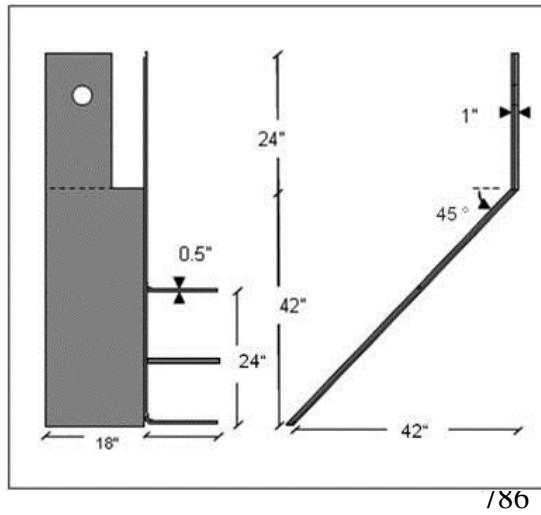
782

783



784

785 **Figure 1** Fiber Optic transect location in the field.

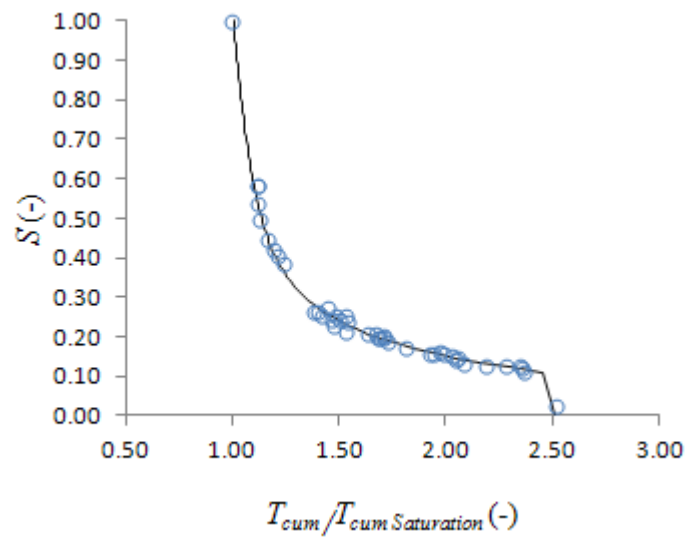


787

(a)

(b)

788 Figure 2 (a) 45-degree “lift-plow” cable insertion tubes design (b) 45-degree “lift-
789 plow” cable insertion tubes.



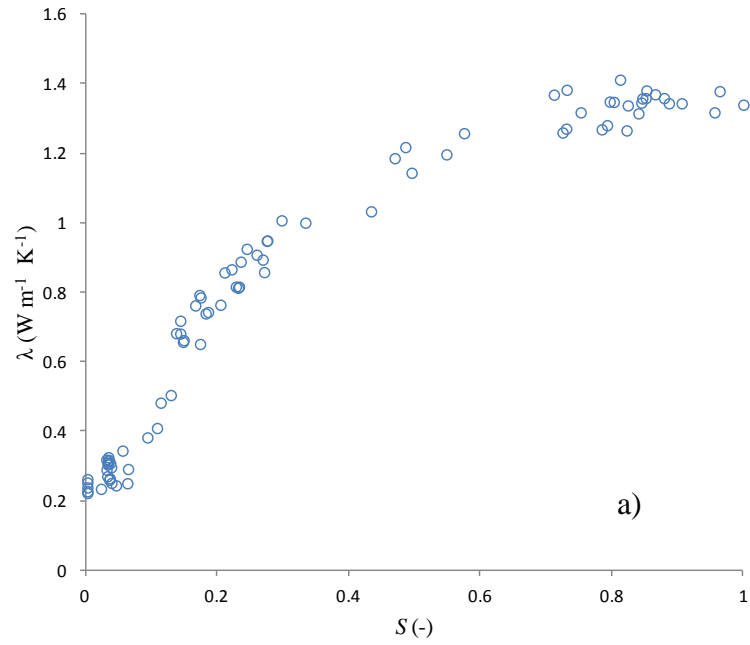
790

791 **Figure 3** Calibration curve relating the degree of saturation (S) to T_{cum} normalized by its value at
792 saturation integrated over 180 seconds for the 1-minute duration heat pulses. The calibration curve has
793 the following form:

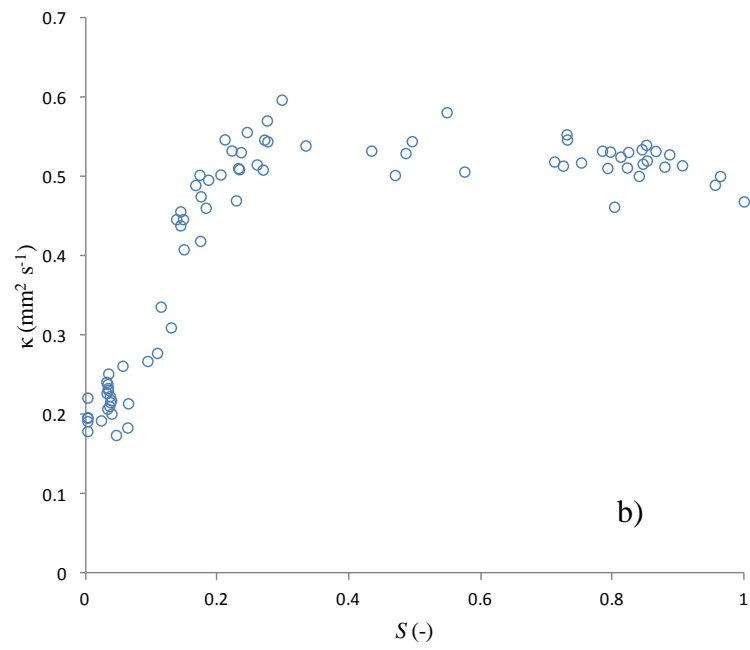
794 $S = 0.0467 + (1.42 + T_{cum}/T_{cum\ Saturation})/(-7.57 + 10.1\ T_{cum}/T_{cum\ Saturation}^2)$ for $S \geq 0.1$

795 and

796 $S = -0.5\ T_{cum}/T_{cum\ Saturation} + 2.51$ for $S < 0.1$



797

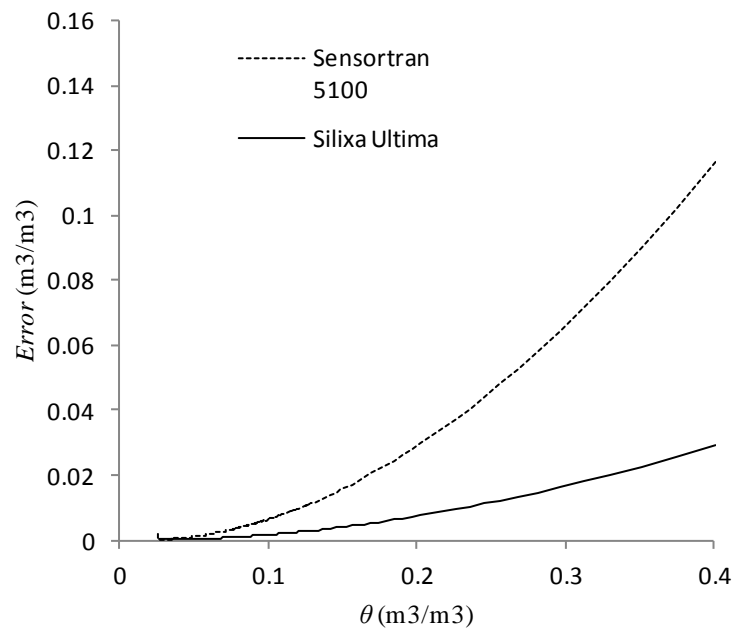


798

799 **Figure 4** Degree of saturation (S) vs. a) thermal conductivity (λ) and b) thermal diffusivity (κ)
 800 measured from non-disturbed samples collected from the calibration soil column. After saturation, the
 801 samples were drained in a pressure chamber to allow measurement of λ at different level of soil water
 802 content using a KD2 Pro sensor.

803

804

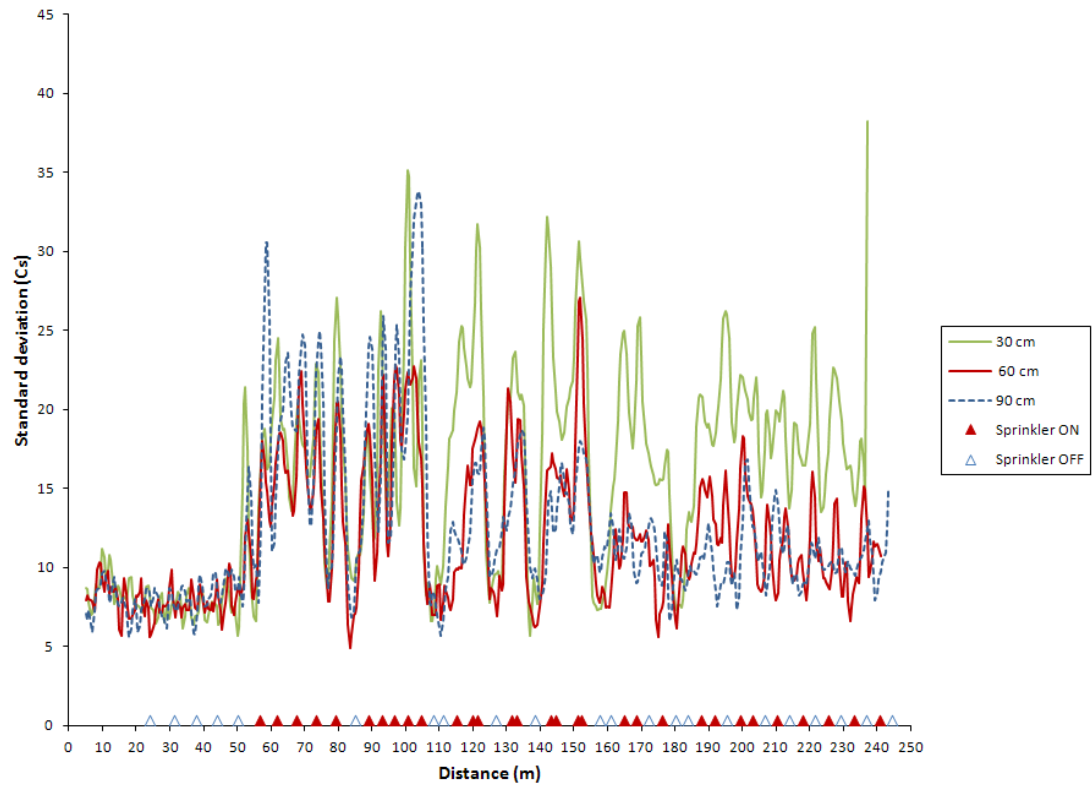


805

806 **Figure 5** Estimated error in soil water content estimation due to the DTS system performance.

807

808



809

810 **Figure 6** Observed standard deviation of T_{cum} at the 30, 60 and 90 cm depths during the 48 hr duration
 811 of the experiment.

812

813

814

815

816

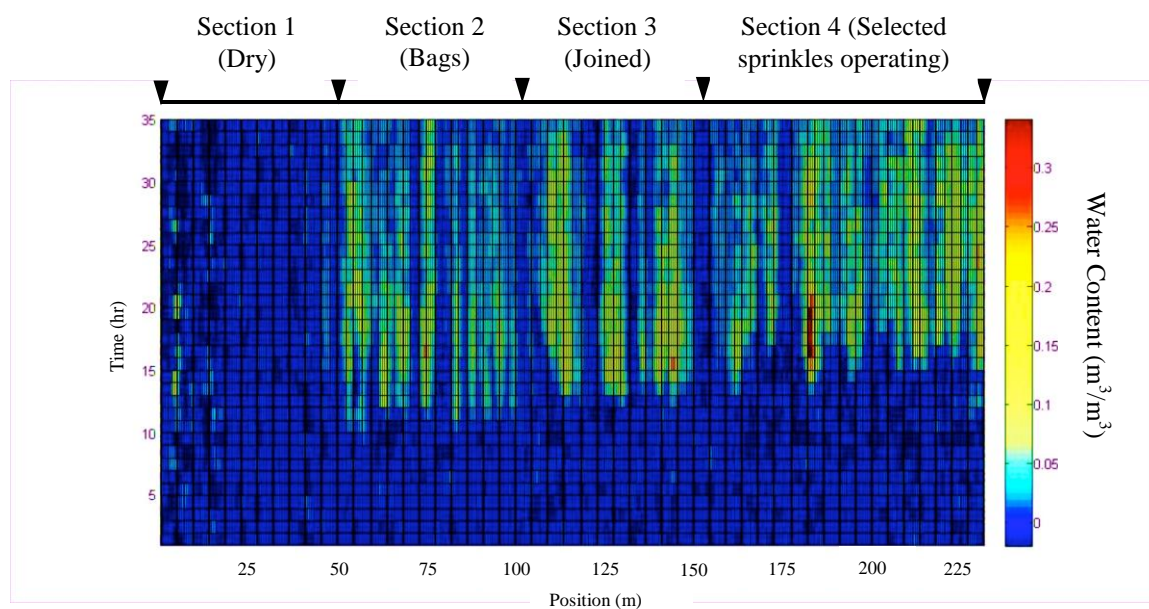
817

818

819

820

821



822

823

824

825

826

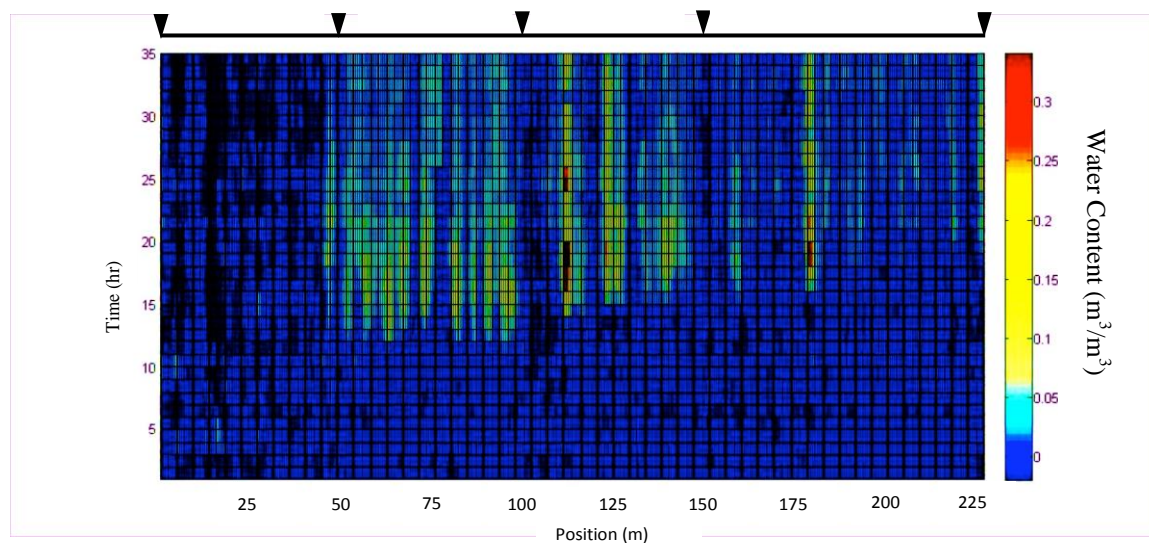
827

828

829

830

831



832

833

834

835

Figure 7 Soil water content change at the 30 cm (top figure) and 60 cm depths (bottom figure).

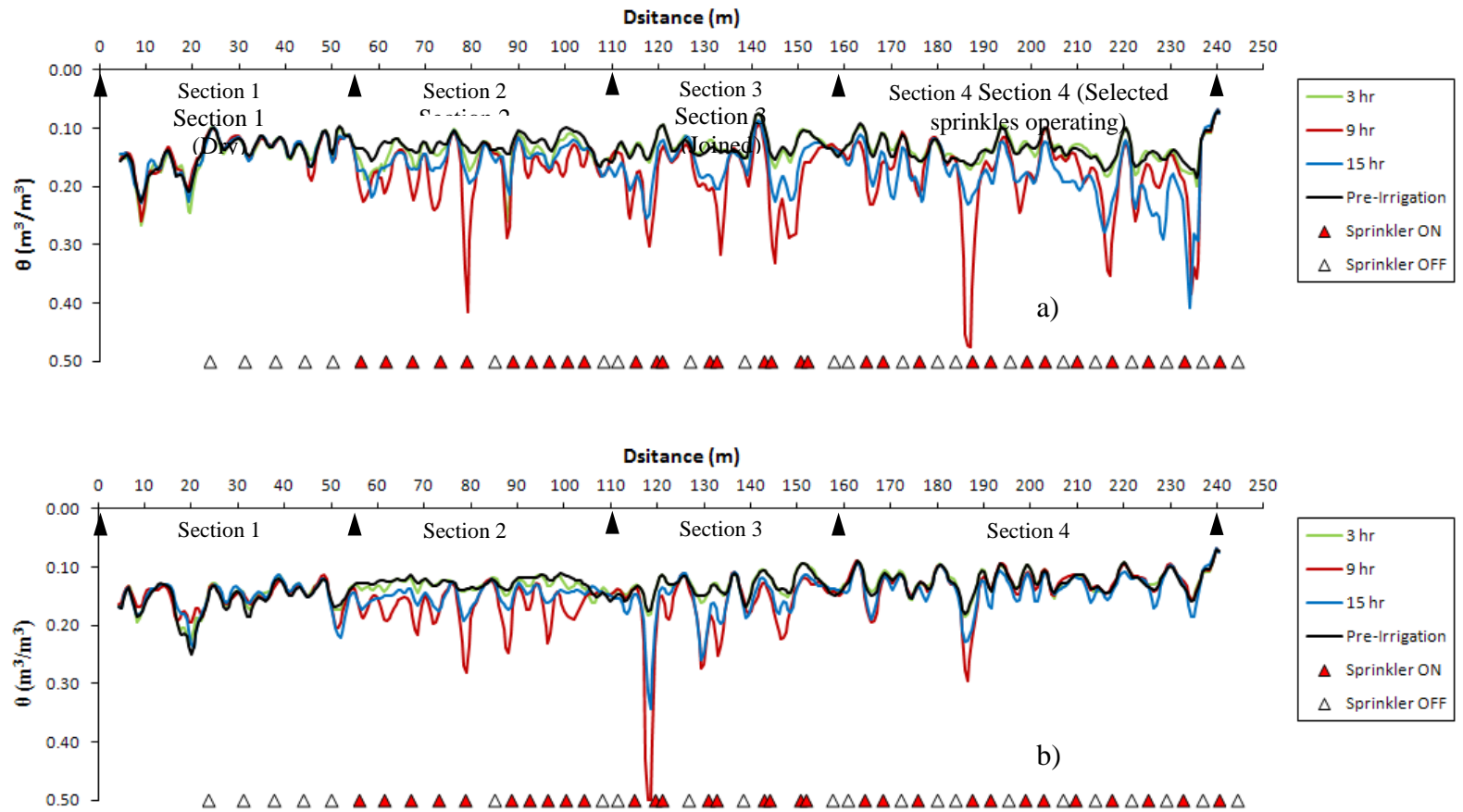


Figure 8 DTS estimated soil water content at a) 30 cm depth and b) 60 cm depth with emitter positions shown before , and at 3, 9, and 15 hours after the 7 hr irrigation set started.

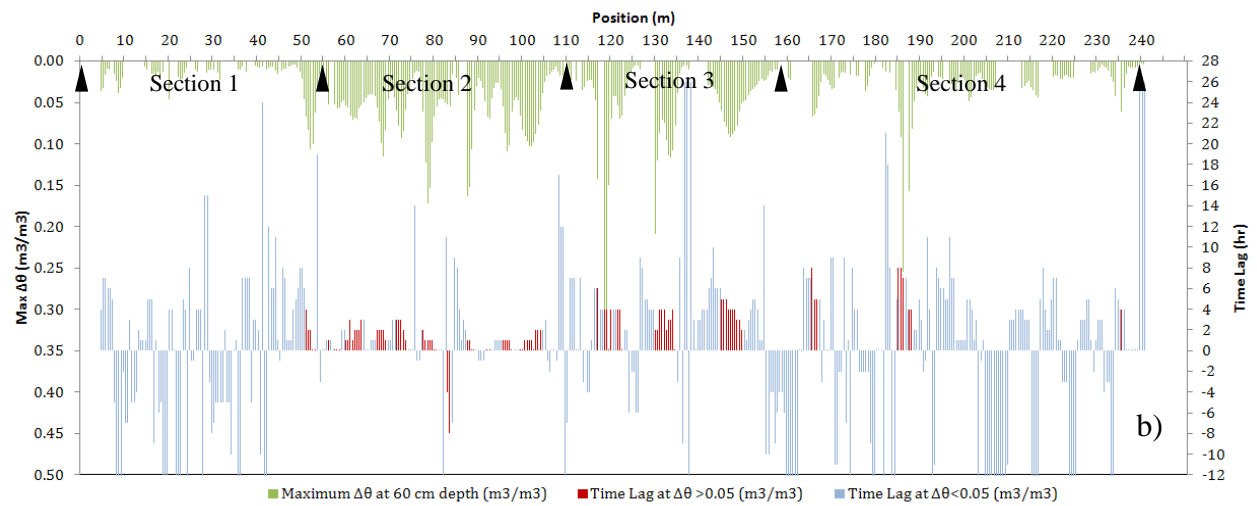
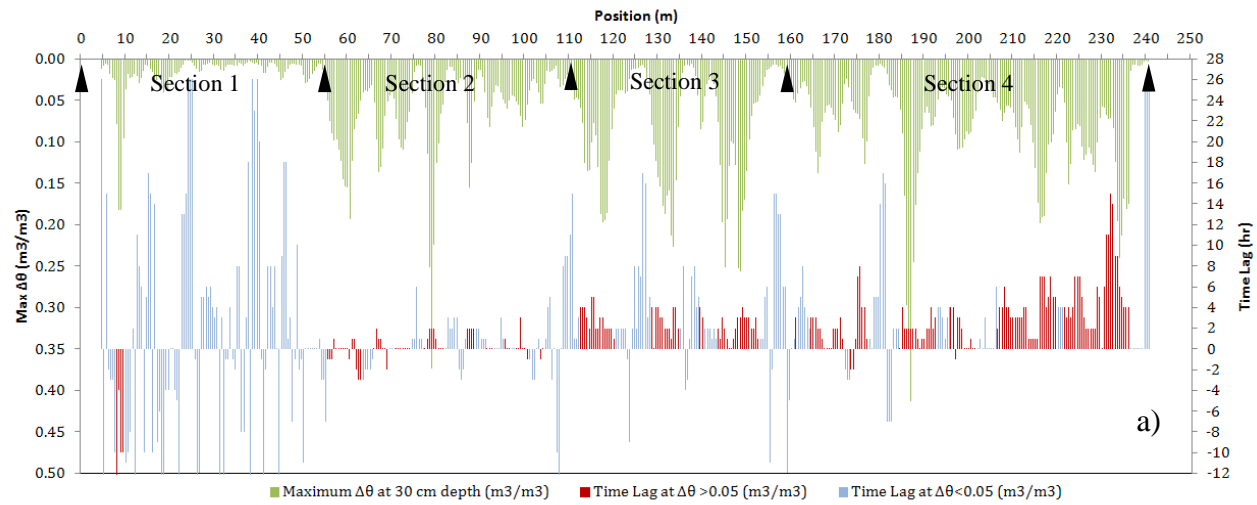


Figure 9 Time lag at the highest time-lagged correlation value a) between $\Delta\theta$ at 30cm and $\Delta\theta$ at 60 cm and b) between ΔT_{cum} at 60cm and ΔT_{cum} at 90 cm

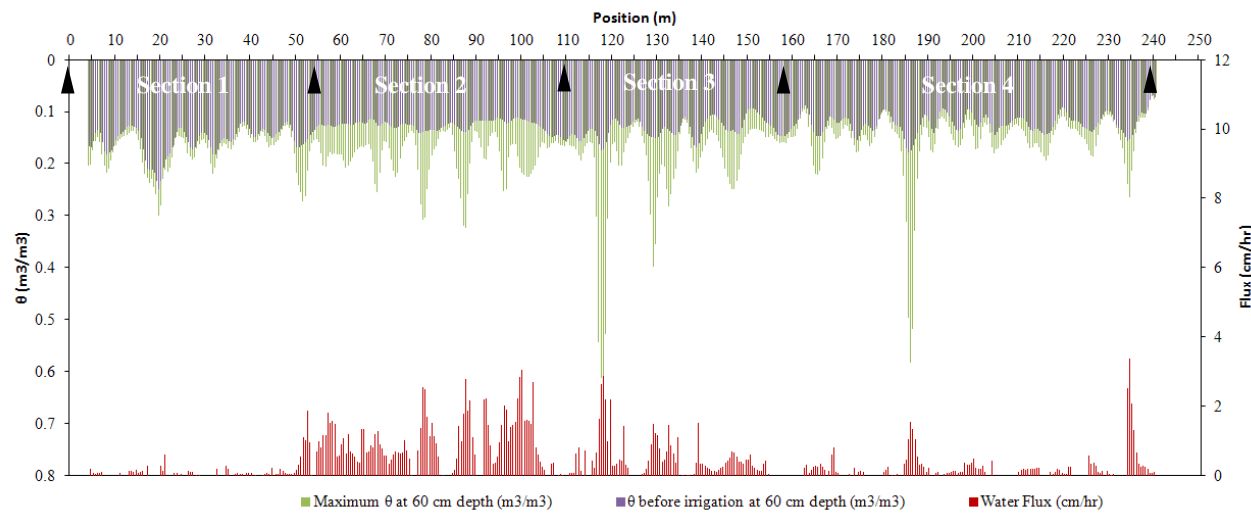
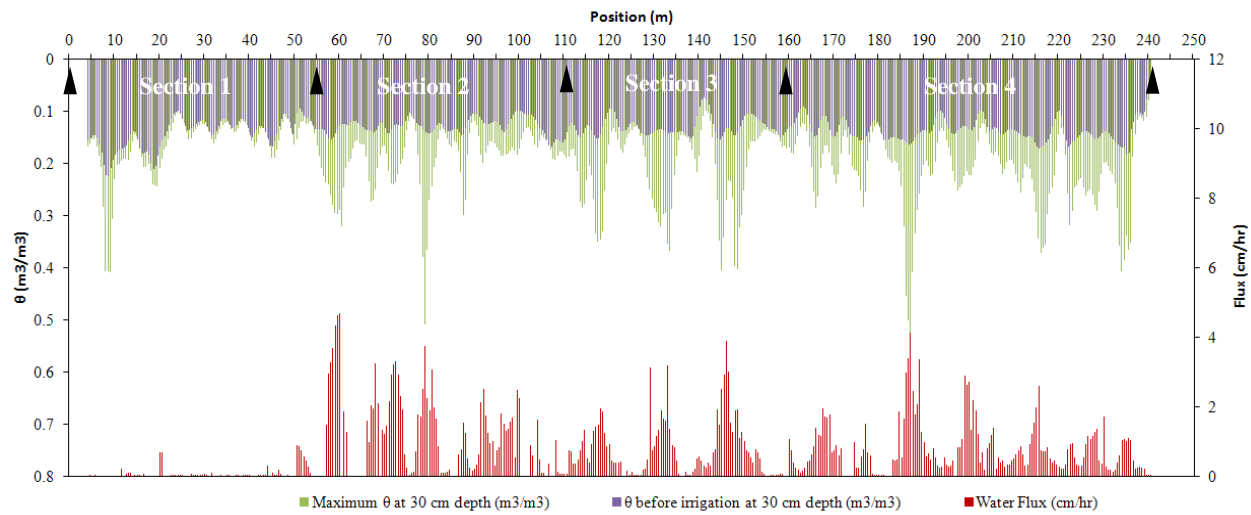


Figure 10 Water flux, pre-irrigation soil water content, and maximum soil water content at the 30 cm depth (top figure), and at the 60 cm depth (bottom figure)

1

2 **Table 1** Soil physical and hydraulic properties (USDA Natural Resources Conservation Service, 2006).

Depth	Bulk density	Sat. Hydr.	Available	Organic matter
(cm)	(g cm ⁻³)	Conductivity m s ⁻¹	Water capacity (cm ³ cm ⁻³)	(%)
0-10	1.15-1.30	14.4-50.4 10 ⁻⁶	0.14-0.17	0.7-1.0
10-89	1.20-1.50	14.4-50.4 10 ⁻⁶	0.14-0.17	0.0-1.0
89-152	1.40-1.70	14.4-50.4 10 ⁻⁶	0.14-0.17	0.0-1.0

3

4

5 **Table 2** Lower bounds on averages fluxes (cm h⁻¹), by section, at 30 and 60 cm depths.

	Section 3			Section 4		
	$\Delta\theta \geq 0.5$ m ³ m ⁻³	$\Delta\theta < 0.5$ m ³ m ⁻³	All locations	$\Delta\theta \geq 0.5$ m ³ m ⁻³	$\Delta\theta < 0.5$ m ³ m ⁻³	All locations
Average Flux at 30 cm depth (cm h ⁻¹)	>1.3	>0.2	>0.8	>0.9	>0.2	>0.8
Average Flux at 60cm depth (cm h ⁻¹)	>1.1	>0.3	>0.5	>1.0	>0.1	>0.2
Average Flux applied at the surface (cm h ⁻¹)	-	-	1.0	-	-	0.8

6

7

8